Compatibility of wind and solar energy with electricity demand in Argentina

Tomás Guozden [*1], Emilio Bianchi [†2], Andrés Solarte[3], and Juan Pablo Carbajal[4]

[1,2]Universidad Nacional de Río Negro, Bariloche
[3]CONAE Comisión nacional de actividades espaciales, Córdoba
[4]Eawag - Swiss Federal Institute of Aquatic Science and Technology, Switzerland

Abstract

One of the greatest obstacles in the exploitation of wind and solar resources is the uncertainty in their availability, usually known as intermittency effects. These effects can be greatly diminished by combining wind and solar resources from different locations. In this article we study the temporal variability of solar irradiance and wind speeds in Argentina, focusing on current projects and those included in GENREN and RENOVAR tenders. We also converted two year wind speeds and irradiance time series into power production, analyzing its compatibility with demand. Finally we numerically search the best distribution of additional capacity that minimizes a basic measure of the intermittency effect.

Resumen

La falta de certeza en la disponibilidad es uno de los mayores obstáculos que se presentan a la hora de aprovechar las energías eólica y solar. Esta característica, usualmente conocida como efectos de intermitencia, puede ser mitigada integrando ambas fuentes y en distintos sitios. En este trabajo estudiamos la variabilidad temporal del recurso eólico y solar en Argentina, enfocándonos en los proyectos ofrecidos en las licitaciones GENREN y RENOVAR. Luego convertimos las series temporales horarias de viento y sol en potencia, durante el perído 2015-2016, estudiando como hubiera sido el recurso de los parques eólicos y solares operativos y próximos a entrar en servicio. Por último analizamos la mejor distribución de potencia adicional a la proyectada tal que su impacto sobre la intermitencia sea mínimo.

[*]tguozden@unrn.edu.ar
[†]ebianchi@unrn.edu.ar

Introduction

Worldwide, energy systems are likely to become more dependent on weather due to the growing share of renewable power sources such as wind and solar [58, 59, 16, 53]. Wind power production exhibits variations on all timescales [1, 20]. Van Der Hoven [55] identified three distinct peaks of wind speeds variability and their most important timescales: i) the turbulent peak in the subsecond to minute range, ii) the diurnal peak, driven by the heating and cooling of the earth surface, and iii) the synoptic peak which depends on changing weather patterns with a scale of variation which ranging from days to weeks [40, 8, 16]. Annual and inter-annual (or decadal) represent important peaks of variability as well [47, 27]. Thus, the variability of wind power production might be classified into regular cycles (diurnal and seasonal/annual), and irregular cycles (synoptic, inter-annual). In constrast to wind speed, solar irradiation presents more defined annual and daily cycles [8]. The observable irregular variations (synoptic and inter-annual) are related to the movement and persistence of clouds and to temperature gradients and drifts.[17, 19, 36, 32]. In addition, the system load usually shows well defined an-

nual, daily and weekly cycles [57, 8] plus inter-annual and weekly variations [57, 60] associated with economic activity and changing weather patterns.

For the reasons described above, the integration of these resources into a power grid may affect several stages of its operation and planning, such as the load frequency control (within the second to minute range), the load following operations (within the minutes to hours range) and the unit commitment scheduling (over the weekly timescale). It may increase the margin of spinning reserves to protect the system against sudden load or renewable power generation fluctuations and the need for flexibility in order to cope with higher ramping rates [58, 50, 40, 59, 24]

Besides the temporal variations described above, wind and solar resources also fluctuate geographically [58]. Studying these spatial variations of the wind and solar outputs is important for two reasons. Firstly, the aggregation of disperse intermittent power sources reduce their overall variability [3, 57, 31, 11, 21, 59, 38]. Secondly, it may help to optimize the complementarity between different renewable power sources and the system load. [58, 59, 38, 16]

The smoothing effect from geographical dispersion has been widely studied for wind power [57, 18, 59]. It is well known that a wider geographical distribution of wind farms reduce their overall variability [35, 46, 13]. This smoothing effect is proportional to the size of the catchment area [2], since the correlation between wind patterns decrease as the distance between sites increase [56, 47]. In contrast, fewer studies have addressed the effect of the dispersion of solar generation [59]. Several studies show that there is also a smoothing effect on the aggregation of dispersed solar power units, but less pronounced than for wind power [29, 36, 11, 59].

Studying the complementarity of different renewable sources (along with the system load) is a complex matter. Some authors claim that solar generation, in contrast with wind generation, usually correlates better with demand over the diurnal [58, 40, 8] and seasonal timescales [58] because it shows well defined cycles. The correlations between wind generation and power demand, on the contrary, are less certain and site-dependent. Therefore, the managerial implications might be different depending on the timescale that is analyzed, since wind and solar generation, and system load timeseries show distinct temporal behaviors [8]. Holttinen [20] found different seasonal and daily average variations in wind power production over distinct regions in Europe. Grams [16] suggested that deploying wind farms in the Balkans instead of the North Sea would reduce synoptic-scale fluctuations over Europe. Heide [18] proposes an optimal seasonal mix of 55% wind and 45% solar generation for Europe since wind correlates better with the seasonal load curve than solar generation. Coker [8] also found that wind generation in UK correlates better with the seasonal load curve than solar generation. Finally, Widen [59] and Monforti [38] studied the complementarity over different timescales of wind and solar generation over Sweden and Italy, respectively. They found negative distance independent correlations between solar and wind power over all timescales, but stronger for monthly averages.

The aim of this article is to assess the complementarity of wind and solar generation over Argentina and its compatibility with demand. Argentina has an appreciable potential for wind and solar power generation [23, 10, 34, 12]. The share of wind and solar power is likely to increase in the incoming years. Law 27191 signed in 2015 has set targets to the share of renewable energies (which also account for biomass, biogas and small hydraulic exploitations): the country is committed to rise the share of renewables up to 12% for the year 2019, and up to 20% by the year 2025. Several tenders have been celebrated: 1470 MW of solar and 3020 MW of wind power were awarded with PPA (power purchase agreement) contracts up to RENOVAR 2.0. Also, other drivers encourage growth of wind and solar power along with tenders. Private initiatives currently account over 500MW, and recently the law to regulate distributed generation has been approved, which leaves place to distributed rooftop photovoltaic generation. Besides the high quality of the wind solar power resources, Argentina has the additional advantage of its wide geographical extension which determines the existence of very distinct climatic regimes [43, 15] (and, hence, distinct cloudiness and wind variability patterns) which should be considered when planning the deployment of wind and solar generation facilities. Hence, understanding the properties of local variations of these power sources is crucial for the development, optimization and operation of harvesting infrastructure. In particular, mixing the sources in accordance with the temporal structure of their variations can lead to power

generation following the demand curve. In the first part of this paper we analyzed the spatial variability and complementarity of the current and planned wind and power plants over Argentina. In the second part of the paper we propose an optimization of future deployments of wind and solar facilities that minimizes the dispersion of the residual demand, i.e., demand minus wind and solar generation.

Methodology

This study is focused on resources from wind and solar projects already in service and others that have been offered in the tenders GENREN, RENOVAR 1, RENOVAR 1.5 and RENOVAR 2.0, and resolutions 108/11 and 202/16.This amounts to a total of 46 wind sites and 21 solar sites that are resumed in tables (4) and (5). Their location can be quickly identified using Fig. (1). The distribution of these sites span a great portion of the country where not only there are strong winds or high solar irradiance; but also have proven some degree of feasibility: for instance in terms of proximity to the electric grid, accessibility or environmental impact concerns.

We analyzed wind and solar resources for each site using wind speeds and irradiance data retrieved from the Modern Era Reanalysis for Research and Applications 2 [37] [39] during the 1980-2016 period. This reanalysis dataset has been widely used to assess the integration of renewable energies [6, 41, 42] because of its time resolution of 1 hour in a spatial grid with 0.5^o latitude by 0.625^o longitude resolution. MERRA2 provides short wave ground solar irradiance and top of the atmosphere short wave irradiance; and wind speed is available at 2, 10 and 50 m above the ground. From these values we computed wind speeds at 100 m height (the typical hub-height of current wind generators) assuming a logarithmic wind profile, by regressing wind speed against the logarithm of height according to the following expression:

$$w(h) = (\frac{u^*}{k}) \log(\frac{h-d}{z}) \quad (1)$$

Where h is the height, u^* is the friction velocity,$k(=0.4)$ is the Von Karman constant, d is the displacement height and z is the surface roughness.

We then simulated two years of power production, using data from reanalysis except for 12 wind park locations where the resource seems to be underestimated by MERRA2 reanalysis. Specifically, we performed the simulations where MERRA2-derived capacity factors were below 0.4 In these sites we performed simulations using the Weather Research and Forecasting (WRF) model. WRF is a state-of-the-art nonhydrostatic high resolution mesoscale model [49, 48]. It was developed (and is regularly updated) by several institutes including the National Center for Environmental Prediction (NCEP) and the National Center for Atmospheric Researches (NCAR). The initial and 6 hour boundary conditions were taken from the Global Forecast System (GFS) operational $0.5^o \times 0.5^o$ resolution global analysis [5, 45]. The outer boundary conditions were updated every 6 hour during the simulation period. Nudging of the solution inside the domain is performed every 12 hours. We implemented two interactive nested domains with grid resolutions of 18 and 6 km and time steps of 90 s and 30 s respectively. The number of vertical levels was set to 55. Vertical levels were placed close together in the low levels and relatively coarsely spaced above. We used the WSM3 [22] and the Thompson [54] microphysics schemes (the latter in the inner domain), the RRTMG long-wave and short-wave physics schemes [26], the MYJ planetary boundary layer scheme [28], the Kain–Fritsch cumulus scheme [30], and the NOAH scheme for land surface physics [7]. An overview of the model domain configuration and physics schemes used are shown in Table 1.

Spatial aggregation and complementarity

We calculated the correlation matrix from the 46 eolic and 21 solar sites, using the hourly data from 1980 to 2017 from MERRA reanalysis both for wind and irradiation. Sites ID are sorted by correlation between themselves, in order to classify them in 10 groups, 9 for wind and solar sites in the 10th group. This grouping of sites was performed ad-hoc, aided with information from the different temporal behavior and distance between them. The results can be seen in Fig. 1.

Then hourly, daily, monthly and annual correlations were calculated as function of distance between a) individual wind farms, b) individual solar farms and c) wind farms and solar farms, to assess the effect of spatial ag-

Table 1: Overview of WRF configuration

Domain 1 N_x x N_y	40 x 39
Domain 1 grid size	16 km
Domain 2 N_x x N_y	16 x 16
Domain 2 grid size	5.33 km
N^o of vertical levels	55
dynamic solver	ARW
period	15 Jan 2015 to 15 Jan 2017
Initial/boundary cond.	NCEP GFS analysis (6h int.)
Microphysics model	Lin et al. scheme
Radiation physics	RRTM scheme
Surface-layer physics	Monin-obukhov (Janjic) scheme
Land-surface physics	Unified Noah LSM
Cumulus physics	Kain-Fritsch (new Eta) scheme
boundary layer option	Mellor-Yamada-Janjic TKE sch.

gregation over different timescales.

The temporal behavior of wind and solar resources were analyzed through daily, monthly and annual heat plots of the solar and wind power outputs.

Wind power production

A simulation of wind and solar power production encompassing a two-year period was performed over the sites described in tables 4 and 5. A similar approach as the Virtual Wind Farm (VWF) model developed in [51, 52] was used to simulate wind power production from wind speeds at 100 m. height, provided by MERRA2 reanalysis and WRF simulations.

Once data at 100 m height was obtained, wind power outputs were computed using power curves of three International Electrotechnical Commission (IEC) classes, according to the mean wind speed at each site. We used three 3.45 MW commercial wind generators power curves:

- Vestas V126 for mean wind speeds below 8 m/s (class IIB – IIIA)
- Vestas V117 for mean wind speeds between 8 and 9.75 m/s (class IEC IB – IIA)
- Vestas V112 for mean wind speeds above 10m/s (class IEC IA)

Before covolving wind speeds with their corresponding power curve, power curves values were smoothed using a gaussian filter, as proposed in the VWFM method.

Solar power production

We used the The Global Solar Energy Estimator (GSEE) developed by Pfenninger and Staffel [42] to calculate the solar power outputs. For each site, the BRL [44, 33] model was applied to obtain direct and diffuse irradiances using the short wave ground-level global irradiance variable SWGDN and top of atmosphere irrandiance SWTDN from the closest MERRA2 grid point. The model then calculates the irradiance on the plane of the solar panels, whether panels are fixed or have tracking capabilities. Skin temperature variable is also used by the model to finally adjust the power output obtained through temperature-efficiency curves, defined by Huld [25].

Optimization of wind and solar plant geographical distribution

In a first attempt to diminish intermittency from overall wind and solar generation, we propose an optimization of the power distribution focusing on the dispersion to mean ratio, namely $\frac{\sigma_R}{\bar{R}}$, where R is the hourly series we are focusing at. If a_i the capacity installed in site i and $w_i(t)$ is the hourly capacity factor of that site (resulting from the virtual wind farm model or solar power) then the hourly power series reads

$$P(t) = \sum_{i=1}^{N} a_i w_i(t), \tag{2}$$

where N are the number of sites or groups used. Additionally, if $D(t)$ is the series of demand then the residual power series is defined as

$$R(t) = D(t) - P(t) = D(t) - \sum_{i=1}^{N} a_i w_i(t), \tag{3}$$

which is the remaining power to be supplied after renewables.

The aim of the optimization problem can be stated as: given a total capacity $C = \sum_i a_i$, find the distribution of

capacity at each site $\{a_i\}$ that minimizes the dispersion of $R(t)$

To solve this problem numerically we extend $w_i(t)$ and a_i variables:

$$\tilde{w}_i(t) = \begin{cases} w_i(t) & \text{for } i = 1, ..., N \\ D(t) & \text{for } i = N+1 \end{cases} \quad (4)$$

and

$$\tilde{a}_i(t) = \begin{cases} a_i(t) & \text{for } i = 1, ..., N \\ -1 & \text{for } i = N+1\,, \end{cases} \quad (5)$$

Then the residual power series can be formulated as

$$R(t) = -\sum_{i=1}^{N+1} \tilde{a}_i \tilde{w}_i(t) \quad (6)$$

Finally we numerically search the distribution of group capacities $\{a_i\}$ that minimizes the dispersion of $R(t)$, forcing the total capacity $\sum_i a_i$ to be constant. We use the relation

$$\text{Var}\left(\sum_i \tilde{a}_i \tilde{w}_i(t)\right) = \sum_{i,j} \tilde{a}_i \tilde{W}_{ij} a_j, \quad (7)$$

where $\tilde{W}_{ij}$ is the covariance between $\tilde{w}_i(t)$ series.

Focusing on dispersion of residual power series is perhaps the simplest way to characterize intermittency. Other methods are for instance studying the ramps plot or hourly variation, or even more sophisticated methods. This work is a first approach to present the problem and characterize interminttence in the region, we hope to analyze more realistic intermittence function costs in the future.

1 Results

Spatial aggregation and complementarity

The correlation matrix for hourly data between 1980-2016 is shown in Fig. 1. Sites 1 and 2 (Arauco and El Sosneado) do not correlate with any other wind site, so each one of them will conform a separate group. Group number 3 gathers the central Argentinian sites, with correlation values between themselves over $r = 0.3$. This is the weakest bonded group, and one of the reasons is the relative longer distances between them compared to other groups. The remaining 6 wind groups are much more correlated, with values over $r = 0.5$. Group 4 extends through the north-eastern part of Buenos Aires province. Group 5 gathers wind parks surrounding Bahía Blanca. Group 6 is located in the eastern region of Río Negro province. Group 7 are parks in the north of Chubut and group 8 are the remaining sites in southern Chubut and Santa Cruz. Group 9 are wind parks located in nearby the border of Río Negro and Neuquén. Finally all solar sites were included in group 10. This classification will be used when optimizing power distribution in the next section.

Figure 2 shows the dependence with distance of hourly, daily, monthly and annual correlations between individual wind farms, individual solar farms and between wind and solar farms. Hourly and daily correlations between wind farms decreases more or less exponentially with distance, with characteristic distances between 1000 km and 1500 km. Monthly and annual correlations between wind farms also decreases with distance, in some cases reaching negative values (up to $r = -0.2$) for distances between 1000 km and 2000 km. This negative correlations indicate the existence of somehow opposing annual/seasonal and interannual behavior of wind speeds.

Solar irradiance time series are mainly dominated by the regular daily and annual cycles. Hourly and monthly correlations show the well defined earth rotating and orbiting cycle, slightly decorrelating with distance due to longitude and latitude incidence in sun altitude. Daily and annual correlations decorrelate much faster with distance, since these series express irregular variations (synoptic scale and interannual) associated with space and time-varying weather patterns.

Contrary to the wind-wind and solar-solar correlations, wind-solar correlations do not show a clear dependence with distance. Instead, the analysis distinguishes between different wind sites. This might be due to the fact that solar irradiance time series are mainly dominated by the regular daily and annual cycles while irregular synoptic and interannual time variations are more important in the wind speed time series.

Most hourly correlations are slightly negative, showing that the daily cycles of solar and wind resources are often desynchronized. Achiras wind farm (center region) shows the highest negative correlations with solar parks (around $r = -0.2$), while Arauco (north-west) shows the highest positive correlations ($r = 0.4$). This feature is analyzed

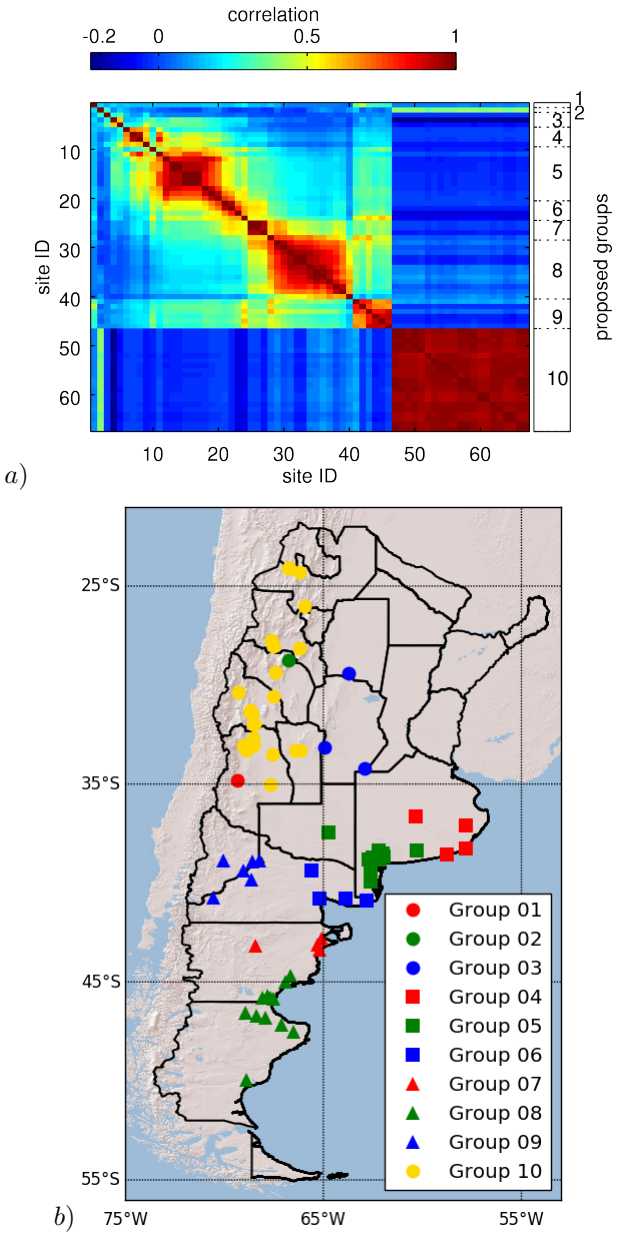

Figure 1: a) Hourly correlation matrix between sites. Proposed groups are shown on the right b) Location of solar (in yellow) and wind (in red, green and blue) sites. This information is available online on `http://dteceolico.unrn.edu.ar/ol3/`

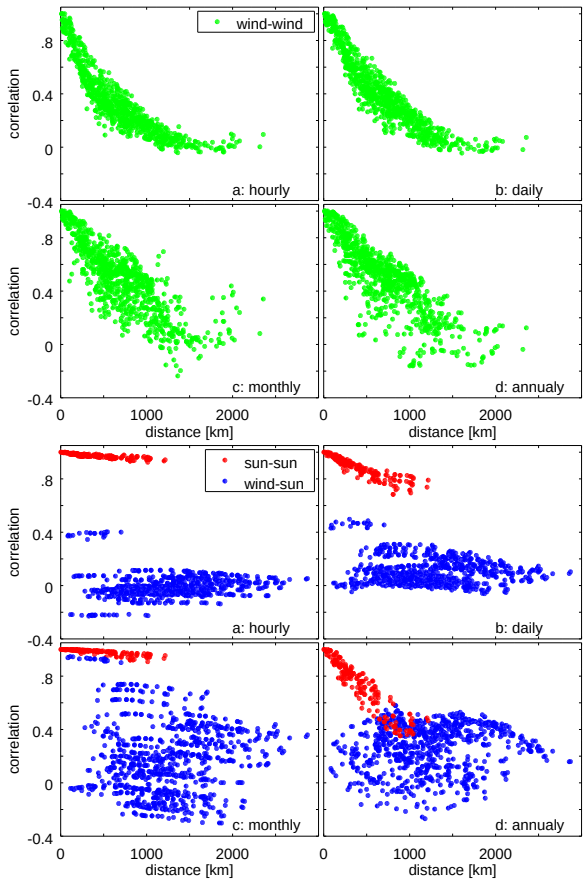

Figure 2: Hourly (a), daily (b), monthly (c) and annual (d) correlations between individual wind farms (green dots), individual solar farms (blue dots) and between wind farms and solar farms (red dots)

in detail in figure 3, which shows the correlation coefficients between the averaged hourly solar irradiances and 100 m height wind speeds at each MERRA2 grid point. Negative correlations dominate in central and eastern Argentina while western and south-easter Argentina shows positive correlations.

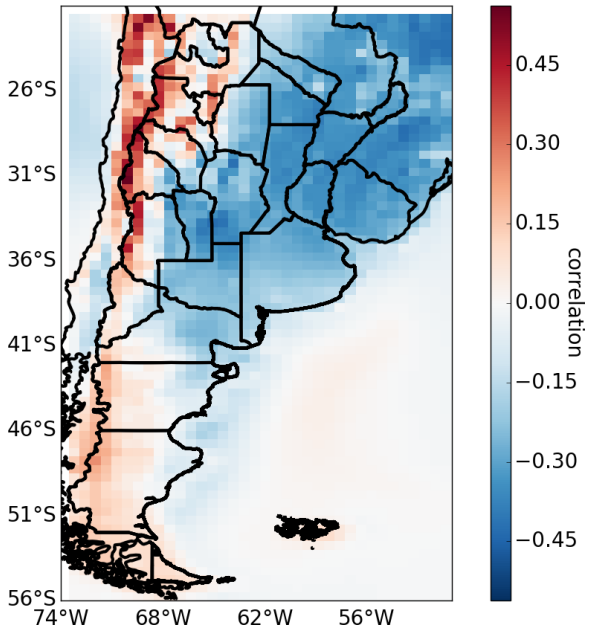

Figure 3: Correlation coefficients (hourly) between 100 m. height wind speeds at each MERRA grid node and averaged solar irradiation at solar sites in table 5)

Daily correlations are positive, most values lying within the $r \in [0, 0.2]$ interval. Arauco, again, shows the stronger positive correlations with solar irradiances (above $r = 0.4$). Monthly and annual correlations show a higher dispersion. Monthly correlations exhibit both positive and negative values, and this reflects the fact that wind speeds show very distinct and sometimes opposing annual/seasonal cycles. Arauco shows the highest correlations with solar irradiances (above $r = 0.9$). The particular behavior of this wind farm might be a consequence of its particular location between two mountain ranges. According to Monforti et al. [38], the Föhn phenomenon on mountainous regions might explain positive correlations between wind speeds and radiation. Finally, annual correlations between wind and solar irradiances are mainly positive, showing that, in general, sunny years match windy years an vice versa. The lack of a clear relation with distance between wind and solar resources could suggest that the smoothing effect of deploying wind and solar plants might not dependent on distance [59]. But currently planned solar plants in Argentina, however, are mostly concentrated in the Cuyo and Northwest regions where the resource is better (Fig. 1). This relation between wind and solar resources might change if solar facilities are installed in other regions and with the expected growth of rooftop generation.

Hourly, monthly and annual plots of the time signals of each individual wind and solar power outputs along with the averaged signal are depicted in Figures 4, 5 and 6. Solar irradiance, as expected, shows a strong daily variation (Fig. 4). It reaches a maximum value that triples the average at around 14:00 local time. Wind power outputs show, instead, a much smaller daily amplitude, with an average range of variation of around $\pm 5\%$ with respect to the average. Broadly, the averaged daily cycle of wind speeds is opposite to the daily cycle of solar irradiance. It shows a minimum at around 10:00, and a maximum at around 21:00. The daily cycles of the different wind farms are much more heterogeneous though. Wind farms located in central Argentina and northeastern Patagonia exhibit two minimums; one during the morning and the other during the afternoon, while wind farms located in southern and western Patagonia exhibit minimum values during the night and morning. Arauco shows a very different daily cycle, with minimum values during the night and morning, and maximum values at around 17:00; and a much more pronounced range of variation (-30% to $+60\%$ with respect to the average).

As with the daily cycle, solar irradiance shows a much stronger annual cycle than wind speeds, with an average range of annual variation of around $\pm 50\%$ with respect to the average (Fig. 5). This is the case when solar panels have 1D or 2D tracking capabilities. In the case of fixed panels maximums occur in autumn and spring equinoxes, and even showing the lowest capacity factor in summer for latitudes below 30^o.

Wind speeds show again, on average, a moderate annual variation ($\pm 5\%$) that is broadly in phase with the annual solar cycle (with lower values during the cold season). However, wind speed shows a noticeable spatial

heterogeneity when analyzed individually. Wind farms located in central Argentina and northeastern Patagonia show an annual cycle contrary to the solar irradiance annual cycle; while Arauco (which also shows a much greater annual amplitude than the rest of the wind farms) and other wind farms located in southern Patagonia, northwestern and eastern Patagonia exhibit an annual cycle that broadly matches the solar annual cycle. Three wind farms located in central Argentina (El Jume, Achiras and Rufino) show maximum values during late winter and spring.

Both wind power and solar resources show noticeable interannual variations, as seen in the yearly array plots in Figure 6. Unlike hourly and monthly averages, the interannual variation of the different wind farms is spatially homogeneous; windy and still years occur simultaneously in broadly all wind farms. On average, the amplitude of wind variations ($\pm 10\%$) is higher than the amplitude of irradiance variations ($\pm 5\%$). It is interesting to note that wind and solar resources show low synchrony from 1980 to approximately 2003, and high synchrony from 2003 to 2017. Wind speeds above the average can be observed in nearly all wind farms during the years 1980, 1990 and 2003. During 2009 and 2010, wind speeds were above the average only in the wind farms located in southern Patagonia. 2016 was a remarkably still year in all wind farms, and specially in those located in Patagonia. This anomaly is related to the persistence of positive Sea Level Pressure (SLP) anomalies over southern Patagonia consistent with the positive phase of the Antarctic Oscillation . Solar irrandiances were above the average during the years 2003, 2009 and 2010 (just as wind speeds), and below the average during 2015 and 2016. This yearly fluctuations in solar irradiances suggest that this variable might be also influenced, through variations in cloudiness, by large-scale climate drivers as El Niño/Southern Oscillation or the AAO [4].

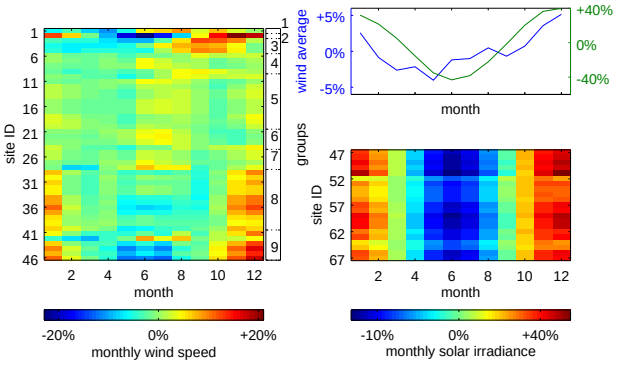

Figure 5: Array plot of monthly individual wind power outputs (left), individual solar power outputs (right) and averaged wind and solar power outputs (upper right). It should be noted that if fixed photovoltaic panels are used, the power series obtained is quite different the solar irradiation annual cycle, with maximums in autumn and spring.

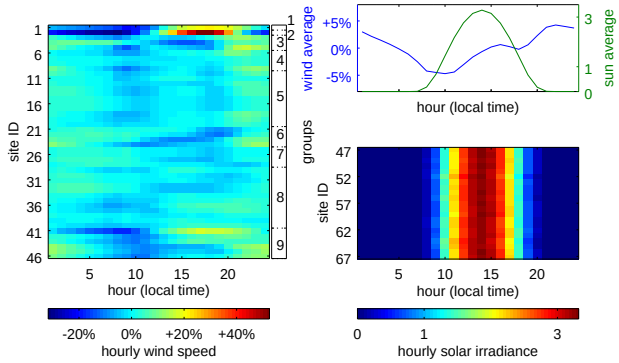

Figure 4: Array plot of hourly individual wind power outputs (left), individual solar power outputs (right) and averaged wind and solar power outputs (upper right)

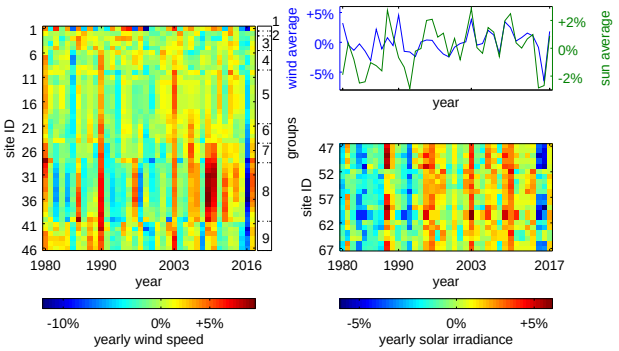

Figure 6: Array plot of yearly individual wind power outputs (left), individual solar power outputs (right) and averaged wind and solar power outputs (upper right)

WRF simulations and conversion of wind and irradiation to power

Several wind power sites clearly seem to be underestimated by MERRA2 reanalisys. We compared MERRA2-derived capacity factors with capacity factors provided by the national grid administrator; the Compañia Administradora del Mercado Mayorista Eléctrico de Argentina (CAMMESA). Regrettably, most of this information is confidential. We perform a downscaling simulation using the WRF model. As we have limited computer capabilities, we chose 12 sites, 11 of them with with MERRA2-derived capacity factotrs below 0.4, as we will see later. Simulations were performed for the period from 2015-01-15 00:00:00 to 2016-01-14 23:00:00.

An example of the model domain used in the WRF simulations is depicted in Fig. 7, in this case for Olavarría wind site, in central Buenos Aires province. Domains 1 and 2 are centered in the point of interest.

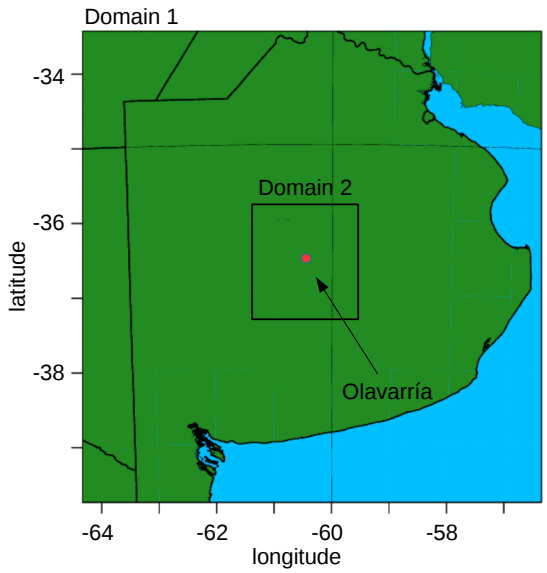

Figure 7: Example of domain used in WRF simulations, in this case for Olavarría (ID number 9). The box inside denotes the second domain with 3 times higher resolution.

MERRA2 wind data and WRF simulations are compared in Table 2. In all cases the mean wind velocity simulated with WRF is higher. A noticeable example is Arauco, where mean velocity obtained with WRF almost doubles the value given by MERRA2. The topography at this location shows a great spatial variability, which is probably not represented by MERRA2 due to its coarse resolution (> 50 km)

Overall correlation and root mean square error of hourly data between results is reasonable, except in Arauco (site 2). We also see for this site that correlation with solar sites is lost, as we indicate in Table 3. Looking at the mean daily wind speed we see that the cycle is delayed by 2 hours (Fig. 8).

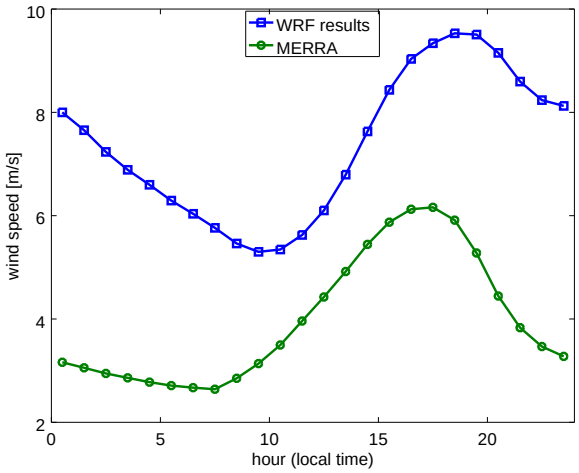

Figure 8: Hourly averages of wind at Arauco, comparing MERRA2 values with WRF simulations

We also computed the weibull k factor for both MERRA2 and WRF hourly data, shown in Table 4. WRF shows lower k values, indicating a higher dispersion in WRF than in MERRA2.

Finally we converted wind speeds and solar irradiation into power outputs using the methods described above, using hourly series from MERRA2 and WRF through years 2015 and 2016. Tables 4 and 5 show the resulting mean capacity factors.

WRF capacity factors are consistently higher than those obtained with MERRA2 reanalysis. We checked the resulting simulated capacity factor of Parque Arauco with the real hourly time series of production during november 2016. This information was again provided by CAMMESA. We supposed an installed capacity of 27

Table 2: Comparison between WRF results for 100 meters wind velocity with MERRA2. Wind velocities obtained by MERRA2 are underestimated in all cases.

id	location	corr	$\bar{v}_{h=100m}$ [m/s]		rmse
			MERRA2	WRF	[m/s]
1	San Rafael	0.61	5.04	8.49	5.23
2	Arauco	0.37	3.98	7.36	3.57
3	El Jume	0.63	6.56	9.91	3.13
4	Achiras	0.42	5.79	8.64	3.94
5	Rufino	0.48	5.72	9.08	4.45
6	Maipú	0.71	7.16	8.80	2.73
9	Olavarría	0.68	6.83	8.59	2.69
10	Gral. Acha	0.66	6.65	8.86	3.05
31	Mles. Behr	0.81	9.88	12.50	3.21
41	Pilcaniyeu	0.71	6.70	8.42	2.80
42	Zapala	0.75	7.24	8.27	3.68
44	Senillosa	0.73	7.05	7.86	2.91

MW. The capacity factor measured using this value is 0.44. Using WRF we obtained a slightly lower capacity factor of 0.41. Using MERRA2 the value for the CF is 0.09, clearly underestimating the site's capacity. The correlation between data is 0.66 and the root mean square error between measured and simulated power is 7.5 MW, which is $\sim 65\%$ of the power average.

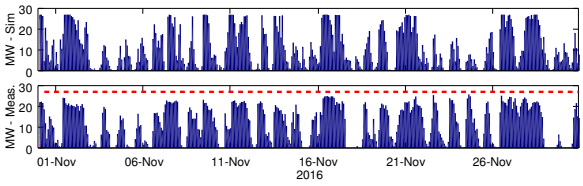

Figure 9: Comparison of hourly measured data from parque Arauco (provided by CAMMESA) and the hourly power series obtained using the Virtual Wind Farm Model[51, 52] and WRF simulations. Installed capacity: 27 MW, measured Capacity Factor: 0.44, simulated capacity factor: 0.41, Correlation: 0.66, RMSE: 7.5 MW

In the case of solar power generation we compared the production obtained from irradiation reanalysis data with the generation of Chimberas Solar Power Plant, a park located in San Juan with 7 MW of polycristalline silicon panels installed capacity, with fixed tilt. This information was also provided by CAMMESA . The comparison is again acceptable, we show the daily values in Figure 10. The capacity factor simulated (0.21) is slightly higher than measured (0.20). Correlation is very high, with an hourly value of 0.93, probably dominated by the daily cycle, as we see when we correlate daily values, obtaining a lower result of 0.69. This can also be seen when calculating the root mean square error: RMSE between hourly data is 48% of mean power, and RMSE between daily values is 23% of mean power.

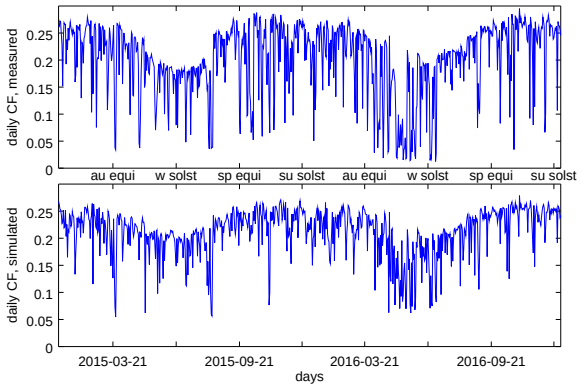

Figure 10: Daily capacity factor of Chimberas solar power plant: Measured, simulated using MERRA2 irradiation data [42]. CF measured capacity factor: 0.20, simulated capacity factor: 0.21, hourly correlation = 0.93, hourly $RMSE = 48\%$ of mean, daily correlation = 0.69, daily $RMSE = 23\%$ of mean.

Maximums of power occur during autumn and spring equinoxes, closely with summer solstices. This is because solar panels are fixed with a tilt of 28^o, which is the value that maximizes the year round capacity factor. Moreeven, for latitudes below 30 degrees summer solstice are the periods with least capacity if fixed panels are used.

1.1 Resources delivered by signed contracts: comparison with demand and future scenarios

Once wind and solar power time series were obtained, we analyzed the overall (solar + wind) power time series of

projected capacity, as described in the last column of Tables 4 and 5. These values correspond to current installed and projected facilities up to RENOVAR 1.5, plus private initiatives in Puerto Madryn and Manantiales Behr, resulting in a total 2458 MW of wind capacity and 924.5 MW for solar capacity (an overall of 3382 MW). These values certainly are subject to variations, as some of the projects remain to be confirmed. We did not add power awarded in RENOVAR 2.0 tender or later.

The resulting total output of the current projected and existing facilities is shown in Fig. 11. Through the years 2015 and 2016 this distribution yielded a capacity factor of 47% for wind parks and 28% from solar parks. The overall capacity factor was 42%, thus delivering 12.4 GWhr per year.

The time series shows maximums between 8hs and 20hs, peaking at 15hs. Monthly average does not show a regular pattern. Winter 2015 and summer 2016/17 are periods of high generation, and the hour of maximum production occurred the 15th of November 2016 at 14:00hs local time, where the hourly capacity factor was as high as 89%.

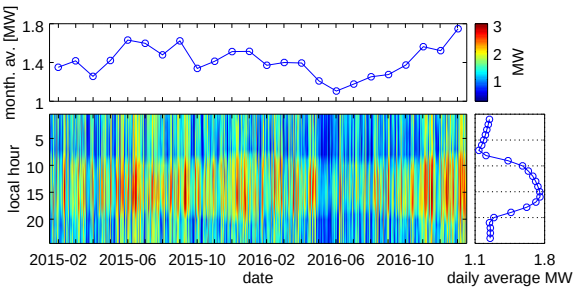

Figure 11: Power series from years 2015 and 2016 of overall 3382.5 MW signed contracts as listed in tables (4,5), consisting of 2458 MW of wind 924.5 MW of solar. The overall capacity factor of 42%, with a coefficient of variation of 37%. Solar sites mean capacity factor is 28% (coefficient of variation 110%) and wind parks mean capacity factor is 47% (coefficient of variation 28%).

On the contrary, both autumns shows minimums. Specially autumn 2016 is an interesting case, where no wind nor sun seemed to be present. In this period the Antarctic Oscillation (AAO) had values much higher than average affecting the weather of most Argentina. Here the hour of minimum production occurred the 18th of May at 7:00hs local time, with an average capacity factor of 6%.

We then compared these power production values with the overall demand throughout the years 2015 and 2016. To do this we use consumption data provided by CAMMESA , which is shown in Fig. (12). Demand shows well defined annual, daily and weekly cycles.

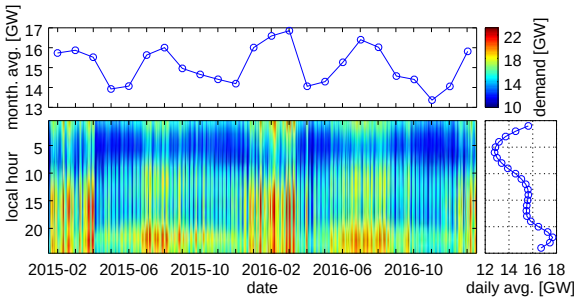

Figure 12: Power series demand from 2015 and 2016, provided by CAMMESA. Average demand is 15.1 GW, with peaks of 23 GW

Analyzing the contribution of current and projected renewable facilities we see that they would have covered 8.7% of demand. We also analyzed the compatibility between renewables and demand. Demand itself has a dispersion equal to $\sigma_{demand} = 2352$ MW. Subtracting the renewable power production during this period yields a residual power series with dispersion $\sigma_{demand-renewables} = 2385$ MW. Also we note that hourly peaks of demand would have been reduced from 23.2 GW to 21.3 GW; and hourly minimum of demand reduces from 9.6 GW to 7.4 GW.

1.2 Adding further renewable capacity: optimizing to diminish intermitency effects

Next we analyzed how to add further wind and solar power capacity, while minimizing intermittence effects. As mentioned above, we have chosen our objective function to be the standard deviation of the residual power series, that are defined as demand minus wind and solar renewables generation. We chose to perform the optimization on the groups described in Fig. 1 instead of individual

Table 3: Some global characteristics from groups: capacity factor, dispersion to mean relation and hourly correlation with the solar group and demand. Groups 2 and 3 are the ones most correlated with demand. Group 3 highly decorrelates with group 10. (Data between 15th of January 2015 and 14th of January 2017)

Group	C.F.	σ/mean	hourly correlation	
			solar gr.	demand
1	0.36	1.01	-0.06	0.09
2	0.41	0.87	-0.06	0.12
3	0.50	0.54	-0.47	-0.12
4	0.47	0.66	-0.17	-0.02
5	0.45	0.62	-0.13	-0.01
6	0.44	0.67	-0.07	-0.03
7	0.46	0.66	-0.09	-0.02
8	0.53	0.58	-0.04	0.00
9	0.43	0.68	-0.17	0.05
10	0.26	1.13	1.00	0.05

facilities. This way allows a more robust method, avoiding possible spurious solutions where most of the power relies in few sites. It also allows the possibility to increase capacity both by adding power to already known sites as well as future new ones at each group, which span almost all of the region.

In Table 3 the mean capacity factor and coefficient of variation for each group is shown, as well as the hourly correlation with demand and group 10 (solar sites).

Groups 10, 1 and 2 are the ones that show the highest variability. Group 2 (Arauco) has the highest correlation with demand, while group 3 is the most anticorrelated. Group 3 is also the most anticorrelated with group 10, with an impressive value of -0.47, in agreement with results shown in Fig. 3.

Now we calculated the optimized distribution of different renewable capacity additions in order to match the residual power (after substracting the production of the current facilities). Results are depicted in Fig. 13 a) and b). Behavior of increasing (or decreasing) capacity with the same distribution as currently projected is shown in dashed lines. The result of adding further capacity, optimizing the distribution between groups is shown in solid lines. We describe three different scenarios of optimized additional capacity: a) (+3.1 GW), b) (+6 GW) and c)

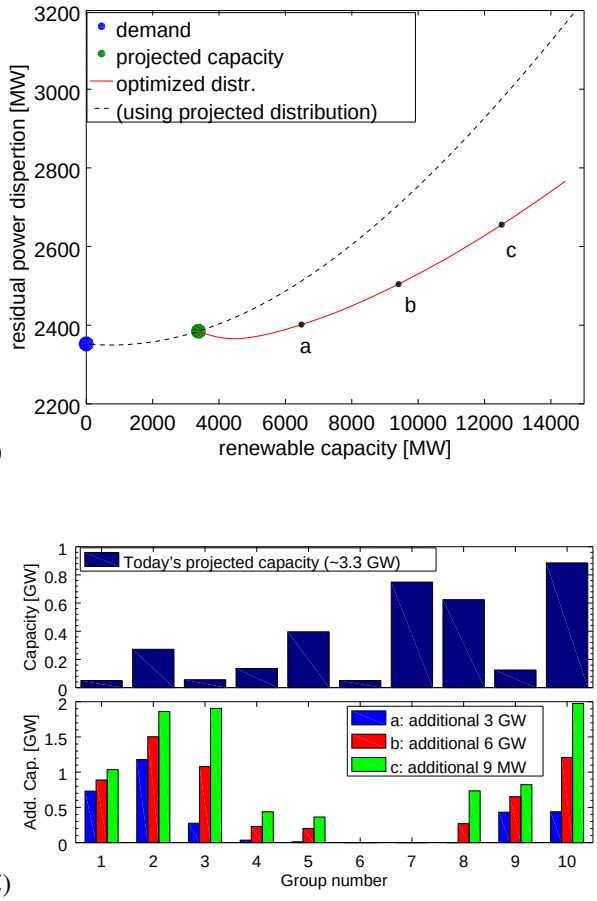

i)

ii)

Figure 13: i) Plot of the standard deviation (σ) of residual power -demand minus renewables- in different scenarios. Dashed lines correspond to capacity with constant distribution as currently projected. Red solid line corresponds to future additional capacity optimized to diminish σ at each value. Three cases (a, b and c) are analyzed below. ii) Power capacity distribution in proposed groups as in Fig. (1). As more renewable capacity is added, wind power in group 3 (which is solar anticorrelated) and solar capacity predominate.

(+9.1 GW), and analyzed the distribution in each one of them.

In a) (blue bars) the optimal solution adds capacity mainly groups 2 and 1, solar sites (group 10) and group 9. This combination yields a mean capacity factor of 0.39. Dispersion of residual power time series results in 2402 MW, slightly above the initial case (2385 MW), showing that up to this range of capacity there is room to compatibilize with current projects and demand.

Optimizing for additional 6 GW of capacity, which is case b) (red bars), still adds power mainly to group 2 (Arauco), closely followed by groups 10 and 3. Also groups 8, 4 and 5 are now considered. Capacity factor is 0.40 and dispersion of residual power increases to 2504 MW. A transition is observed in which dispersion due to added capacity is starting to prevail.

Finally, the best distribution of additional 9 GW (case c, green bars) adds power to groups 10, 3 and 2 mainly ($CF = 0.40$). In this case dispersion is 2656 MW, and increases almost linearly if further capacity is added, showing that new added capacity is distributed mainly to minimize its own dispersion. This explains the amount of capacity added in group 3, anticorrelating the demand but compensating solar sites.

From this analysis we found that, focusing on dispersion only, the penetration of wind and solar facilities may increase up to more or less 3 GW while dispersion almost remains constant. From this point on, optimal distribution focuses in compensating variations between groups. Here group 3 stands out, as it compensates the solar cycle.

In Fig. 14 we plot the hourly averages of demand and groups 3, 2 (Arauco) and 10 (solar sites). Here the anticorrelation of group 3 and solar sites is evident, as it is also the similarity between group 2 (Arauco) and demand.

Another way to analyze intemittency from a signal is looking at the ramps plot. In this the hour to hour change is calculated and with this data an histogram is built, classifying bins according to the magnitude of the change. Information about the smoothness of the series can be obtained from this histogram.

In Fig. 15 we show the ramps plot of demand, the residual power after current projects and three hypothetical cases analyzed in Fig. 13. (Both positive and negative variations are counted together).

There is a rapid increase in the number of events where residual power changes is over 2 GW when renewable ca-

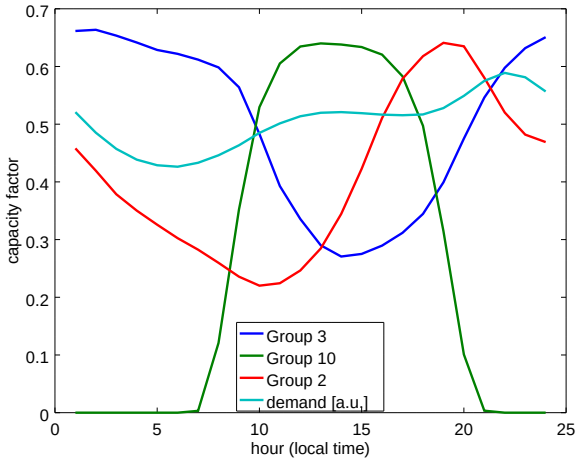

Figure 14: Hourly averages of demand, groups 2 and 3 (from WRF data) and solar sites average (group 10)

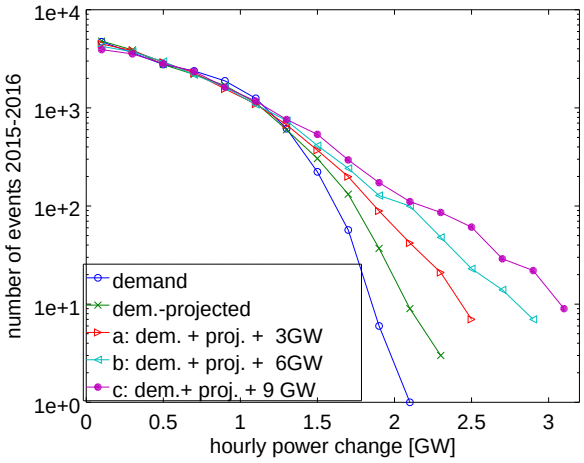

Figure 15: Ramps plot: histogram of hour to hour power change. Circles represent demand by itself. Also the addition of current projected renewables, and case a), b) and c) from Figure (13) are analyzed.

pacity is added. An optimization following this idea could be developed, although it would be much more susceptible to spurious results in simulations.

2 Conclusions

This article analyzed the compatibility of wind and solar resources with demand in Argentina, focusing in specific sites rather than a global study of the region. We chose sites from locations of projects already in operation, projects under construction or those awarded in recent tenders. By working with these sites we assure the most convenient places in terms of resource abundance, electricity grid accessibility and other feasibility concerns. We gathered 46 wind sites and 19 solar sites that span almost all the country.

In the first part of the article we studied correlation and variability at the resource of each site. With this information we separated sites in ten groups, 9 groups of wind sites and a group including all solar sites. Within these groups sites tend to show characteristic hourly, monthly and annual cycle, although there are exceptions.

We found that distance affects correlation mainly between wind parks. In solar sites the hourly and seasonal cycle of the sun prevails, and differences in cloudiness is noticeable when looking at daily averages at some degree, but only annual averages of irradiation are comparable with wind decorrelation with distance.

Hourly, monthly and annual averages of sites show interesting patterns, distinguishable between groups. Many features are found analizing temporal variability, we highlight here the complementarity between solar irradiance and wind in central Argentina (El Jume, Achiras and Rufino), and the great diversity between wind regimes.

Wind and solar power simulations during the years 2015 and 2016, based both on MERRA2 data and WRF simulations. These simulations yielded, for current projects, a capacity factor of 47% for wind parks and 28% for solar parks, resulting in an overall capacity factor of 42%. These facilities would have covered 8.7% of the overall electricity demand in that period. Residual demand (that is demand minus renewables) would have slightly increased its dispersion (2385 MW) if compared with the raw dispersion of demand (2352 MW), showing good compatibility. Hourly peaks of demand would have been reduced from 23.2 GW to 21.3 GW; and hourly minimum of demand from 9.6 GW to 7.4 GW.

An optimization of the distribution of wind and solar facilities was performed for three scenarios of capacity additions a) ($+3$ GW), b) ($+6$ GW) and c) ($+9$ GW). The objective was to minimize the dispersion of the residual demand. From this analysis we found that, focusing on dispersion only, the penetration of wind and solar facilities may increase in an additional of more or less 3 GW while keeping dispersion almost constant. From this point on, optimal distribution starts focusing in compensating variations between groups.

In May 2016 a sharp decrease in resources ocurred. In this period the set current projects would have reduced the mean monthly capacity factor in about $\sim 30\%$ respect to the 2015-2016 average. This suggest a strong connection between resources and the AAO parameter, as pointed out in [4].

Overall there is a huge potential of wind and sun resources in Argentina, and the diversity in temporal behavior allows for great reduction on renewables intemitence. Moreeven, interconnection with Chile Uruguay and Brasil has the potential to mitigate intermittency even further. We will investigate these possibilities in a near future.

References

[1] M. Albadi and E. El-Saadany. Overview of wind power intermittency impacts on power systems. *Electric Power Systems Research*, 80(6):627–632, 2010.

[2] C. L. Archer and M. Z. Jacobson. Supplying baseload power and reducing transmission requirements by interconnecting wind farms. *Journal of Applied Meteorology and Climatology*, 46(11):1701–1717, 2007.

[3] H. Beyer, J. Luther, and R. Steinberger-Willms. 'power fluctuations from geographically diverse, grid coupled wind energy conversion systems. In *European wind energy conference proceedings*, pages 306–310, 1989.

[4] E. Bianchi, A. Solarte, and T. M. Guozden. Large scale climate drivers for wind resource in southern

Table 4: Wind parks installed and projected. Projected power values correspond to tenders up to RENOVAR 1.5, and are supposed to be operative in 2019. Superscript denote the origin of the project: a: current operational (GENREN and Resol. 108/11) b: RENOVAR 1, c: RENOVAR 1.5, d: RENOVAR 2, e : Resol. 202/16, f: private initiatives. WRF values as well as all capacity factors correspond to the period from 2015-01-15 to 2016-01-14. Source: CAMMESA [9] Online at `http://dteceolico.unrn.edu.ar/ol3/`

ID	Gr.	Province	Location	lat	lon	$\bar{v}_{h=100m}$ [m/s]		weibull k		CF		Power
						MERRA	WRF	MERRA	WRF	MERRA	WRF	[MW]
1	1	Mendoza	San Rafael	-34.84	-69.33	5.04	8.49	1.77	1.68	0.19	0.36	^{e}50
2	2	La Rioja	Arauco	-28.75	-66.75	3.98	7.36	2.01	2.00	0.09	0.41	^{a,b,c}272
3	3	S. del Estero	El Jume	-29.42	-63.71	6.56	9.91	3.98	2.70	0.28	0.55	^{a}8
4	3	Córdoba	Achiras	-33.14	-64.96	5.79	8.64	3.11	2.20	0.22	0.46	^{c}48
5	3	Santa Fe	Rufino	-34.20	-62.90	5.72	9.08	3.46	1.80	0.20	0.48	^{b}-
6	4	Buenos Aires	Maipú	-37.10	-57.80	7.16	8.80	3.29	2.45	0.36	0.50	^{b}-
7	4	Buenos Aires	Miramar	-38.27	-57.83	8.29	-	2.63	-	0.45	-	^{c}98
8	4	Buenos Aires	Necochea	-38.56	-58.75	7.92	-	2.84	-	0.46	-	^{c}38
9	4	Buenos Aires	Olavarría	-36.64	-60.34	6.83	8.59	3.09	2.43	0.33	0.49	^{d}-
10	5	La Pampa	Gral. Acha	-37.43	-64.72	6.65	8.86	3.08	2.23	0.31	0.50	^{c}37
11	5	Buenos Aires	Tres Arroyos	-38.82	-60.32	7.75	-	3.06	-	0.44	-	^{b,c}100
12	5	Buenos Aires	Bahía Blanca	-38.61	-62.34	7.84	-	3.02	-	0.45	-	^{b,c,d}-
13	5	Buenos Aires	Cnel. Rosales	-38.71	-62.53	7.87	-	3.02	-	0.45	-	^{c}-
14	5	Buenos Aires	Bahía Blanca	-38.36	-62.21	7.87	-	3.02	-	0.45	-	^{b}10
15	5	Buenos Aires	Tornquist	-38.50	-62.00	8.11	-	3.01	-	0.43	-	^{e}-
16	5	Buenos Aires	Bahía Blanca	-38.62	-62.02	8.11	-	3.01	-	0.43	-	^{b}100
17	5	Buenos Aires	Bahía Blanca	-38.67	-61.96	8.11	-	3.01	-	0.43	-	^{c}-
18	5	Buenos Aires	Villarino	-38.82	-62.70	7.72	-	3.15	-	0.43	-	^{b}99
19	5	Buenos Aires	Buratovich	-39.25	-62.62	7.82	-	3.27	-	0.44	-	^{b}50
20	5	Buenos Aires	Villalonga	-40.03	-62.66	7.93	-	3.18	-	0.45	-	^{a,b}50
21	6	Buenos Aires	Carmen de Pat.	-40.90	-62.83	8.14	-	2.91	-	0.44	-	^{b}-
22	6	Río Negro	Adolfo Alsina	-40.80	-63.87	8.14	-	2.79	-	0.44	-	^{c}-
23	6	Río Negro	San Antonio	-40.80	-65.20	7.74	-	2.48	-	0.44	-	^{b}-
24	6	Río Negro	Choele Choel	-39.35	-65.59	7.50	-	2.88	-	0.41	-	^{c}100
25	7	Chubut	Trelew	-43.12	-65.26	8.58	-	2.68	-	0.48	-	^{a,b,c}248
26	7	Chubut	Puerto Madryn	-42.83	-65.08	8.58	-	2.68	-	0.48	-	^{f}300
27	7	Chubut	Rawson	-43.35	-65.18	8.47	-	2.46	-	0.47	-	^{a}101
28	7	Chubut	Gastre	-42.38	-69.28	9.73	-	2.45	-	0.53	-	^{b}-
29	8	Chubut	Garayalde	-44.71	-66.73	8.97	-	2.89	-	0.50	-	^{b}24
30	8	Chubut	Malaspina	-44.92	-66.99	9.30	-	2.77	-	0.51	-	^{e}50
31	8	Chubut	Mles. Behr	-45.67	-67.81	9.88	12.50	2.58	2.40	0.55	0.69	^{b,d,f}100
32	8	Chubut	C. Rivadavia	-45.85	-67.50	9.54	-	2.35	-	0.52	-	^{a}3
33	8	Chubut	C. Rivadavia	-45.78	-67.67	9.54	-	2.35	-	0.52	-	^{a}6
34	8	Chubut	P.del Castillo	-45.79	-68.06	9.58	-	2.49	-	0.53	-	^{b}24
35	8	Santa Cruz	Koluel Kaike	-46.70	-68.40	9.13	-	2.52	-	0.51	-	^{e}220
36	8	Santa Cruz	Las Heras	-46.55	-68.95	9.05	-	2.45	-	0.50	-	^{b}97
37	8	Santa Cruz	Pico Truncado	-46.82	-67.94	8.62	-	2.68	-	0.47	-	^{c}-
38	8	Santa Cruz	Jaramillo	-47.18	-67.14	8.89	-	2.76	-	0.50	-	^{c}100
39	8	Santa Cruz	Puerto Deseado	-47.55	-66.18	9.06	-	2.94	-	0.52	-	^{b}-
40	8	Santa Cruz	Piebra Buena	-50.06	-69.12	9.02	-	2.56	-	0.51	-	^{c}-
41	9	Río Negro	Pilcaniyeu	-40.73	-70.58	6.70	8.42	2.13	2.32	0.32	0.46	^{b}50
42	9	Neuquén	Zapala	-38.86	-70.05	7.24	8.27	2.18	1.69	0.36	0.39	^{b}-
43	9	Río Negro	Cerro Policía	-39.83	-68.63	7.94	-	2.56	-	0.44	-	^{b}-
44	9	Neuquén	Senillosa	-38.93	-68.56	7.05	7.86	2.12	1.80	0.37	0.45	^{b}-
45	9	Neuquén	Confluencia	-38.87	-68.23	7.41	-	2.37	-	0.40	-	^{b}75
46	9	Neuquén	Picún Leufú	-39.36	-69.04	7.48	-	2.23	-	0.41	-	^{b}-

Table 5: Solar park projects awarded in RENOVAR 1 and RENOVAR 1.5 tenders. All projects are located in the Northwest region of Argentina, where the mean irradiances above 200 W/m^2, over 300 W/m^2 in two cases. Chimberas (fixed panels) and San Juan 1 [14] (fixed, 1D and 2D tracking panels) are already operational projects. The rest of the projects have 1D tracking panels except Cachaurí with fixed panels. Source: CAMMESA [9]

ID	Name	Province	lat	lon	$\bar{Irr}$ [W/m^2]	CF	Power [MW]
47	Lavalle	MENDOZA	-32.71	-68.52	249	0.25	17.60
48	Lujan de Cuyo	MENDOZA	-33.07	-69.05	244	0.24	22.00
49	La Paz	MENDOZA	-33.48	-67.56	238	0.23	14.08
50	PASIP	MENDOZA	-33.04	-68.54	244	0.24	1.15
51	General Alvear	MENDOZA	-35.04	-67.66	232	0.23	17.60
52	Cafayate	SALTA	-26.03	-65.94	284	0.32	80.00
53	Nonogasta	LA RIOJA	-29.33	-67.42	262	0.27	35.00
54	Fiambala	CATAMARCA	-27.74	-67.64	283	0.31	11.00
55	Tinogasta	CATAMARCA	-28.04	-67.54	268	0.28	15.00
56	Saujil	CATAMARCA	-28.16	-66.22	264	0.27	22.50
57	Sarmiento	SAN JUAN	-31.97	-68.48	254	0.26	35.00
58	Anchoris	MENDOZA	-33.31	-68.89	259	0.26	95.50
59	Caldenes del Oeste	SAN LUIS	-33.30	-66.39	242	0.24	21.30
60	La Cumbre	SAN LUIS	-33.32	-66.17	234	0.24	24.75
61	Ullum	SAN JUAN	-31.30	-68.67	234	0.24	22.00
62	Iglesia- Guañizuli	SAN JUAN	-30.34	-69.27	280	0.31	80.00
63	Las Lomitas	SAN JUAN	-30.59	-67.52	255	0.26	1.70
64	La Puna	SALTA	-24.27	-66.20	304	0.35	100.00
65	Cauchari	JUJUY	-24.10	-66.73	313	0.27	300.00
66	Chimberas	SAN JUAN	-31.99	-68.54	246	0.20	7
67	San Juan 1	SAN JUAN	-31.39	-68.68	246	0.22	1.2

south america. *Renewable Energy*, 114:708–715, 2017.

[5] K. Campana, P. Caplan, J. Alpert, et al. Technical procedures bulletin for the t382 global forecast system. 2005.

[6] D. Cannon, D. Brayshaw, J. Methven, P. Coker, and D. Lenaghan. Using reanalysis data to quantify extreme wind power generation statistics: a 33 year case study in great britain. *Renewable Energy*, 75:767–778, 2015.

[7] F. Chen and J. Dudhia. Coupling an advanced land surface–hydrology model with the penn state–ncar mm5 modeling system. part i: Model implementation and sensitivity. *Monthly Weather Review*, 129(4):569–585, 2001.

[8] P. Coker, J. Barlow, T. Cockerill, and D. Shipworth. Measuring significant variability characteristics: An assessment of three uk renewables. *Renewable energy*, 53:111–120, 2013.

[9] Compañía administradora del mercado mayorista eléctrico. `http://www.cammesa.com.ar/`.

[10] B. J. De Vries, D. P. Van Vuuren, and M. M. Hoogwijk. Renewable energy sources: Their global potential for the first-half of the 21st century at a global level: An integrated approach. *Energy policy*, 35(4):2590–2610, 2007.

[11] M. A. Delucchi and M. Z. Jacobson. Providing all global energy with wind, water, and solar power, part ii: Reliability, system and transmission costs, and policies. *Energy policy*, 39(3):1170–1190, 2011.

[12] E. Dupont, R. Koppelaar, and H. Jeanmart. Global available wind energy with physical and energy return on investment constraints. *Applied Energy*, 209:322–338, 2018.

[13] C. Fant, B. Gunturu, and A. Schlosser. Characterizing wind power resource reliability in southern africa. *Applied Energy*, 161:565–573, 2016.

[14] P. Gambetta and V. M. Doña. Planta solar fotovoltaica san juan 1: Descripción de se diseño y detalles de operación. *Cuarto Congreso Nacional – Tercer Congreso Iberoamericano Hidrógeno y Fuentes Sustentables de Energía – HYFUSEN 2011*, 2011.

[15] R. D. Garreaud, M. Vuille, R. Compagnucci, and J. Marengo. Present-day south american climate. *Palaeogeography, Palaeoclimatology, Palaeoecology*, 281(3):180–195, 2009.

[16] C. M. Grams, R. Beerli, S. Pfenninger, I. Staffell, and H. Wernli. Balancing europe's wind-power output through spatial deployment informed by weather regimes. *Nature climate change*, 7(8):557, 2017.

[17] C. A. Gueymard and S. M. Wilcox. Spatial and temporal variability in the solar resource: Assessing the value of short-term measurements at potential solar power plant sites. In *Solar 2009 ASES Conf*, 2009.

[18] D. Heide, L. Von Bremen, M. Greiner, C. Hoffmann, M. Speckmann, and S. Bofinger. Seasonal optimal mix of wind and solar power in a future, highly renewable europe. *Renewable Energy*, 35(11):2483–2489, 2010.

[19] T. E. Hoff and R. Perez. Quantifying pv power output variability. *Solar Energy*, 84(10):1782–1793, 2010.

[20] H. Holttinen. Hourly wind power variations in the nordic countries. *Wind energy*, 8(2):173–195, 2005.

[21] H. Holttinen, P. Meibom, A. Orths, B. Lange, M. O'Malley, J. O. Tande, A. Estanqueiro, E. Gomez, L. Söder, G. Strbac, et al. Impacts of large amounts of wind power on design and operation of power systems, results of iea collaboration. *Wind Energy*, 14(2):179–192, 2011.

[22] S.-Y. Hong, J. Dudhia, and S.-H. Chen. A revised approach to ice microphysical processes for the bulk parameterization of clouds and precipitation. *Monthly Weather Review*, 132(1):103–120, 2004.

[23] M. Hoogwijk, B. de Vries, and W. Turkenburg. Assessment of the global and regional geographical, technical and economic potential of onshore wind energy. *Energy Economics*, 26(5):889–919, 2004.

[24] M. Huber, D. Dimkova, and T. Hamacher. Integration of wind and solar power in europe: Assessment of flexibility requirements. *Energy*, 69:236–246, 2014.

[25] T. Huld, R. Gottschalg, H. G. Beyer, and M. Topič. Mapping the performance of pv modules, effects of module type and data averaging. *Solar Energy*, 84(2):324–338, 2010.

[26] M. J. Iacono, J. S. Delamere, E. J. Mlawer, M. W. Shephard, S. A. Clough, and W. D. Collins. Radiative forcing by long-lived greenhouse gases: Calculations with the aer radiative transfer models. *Journal of Geophysical Research: Atmospheres*, 113(D13), 2008.

[27] N. Isyumov. Alan g. davenport's mark on wind engineering. *Journal of Wind Engineering and Industrial Aerodynamics*, 104:12–24, 2012.

[28] Z. I. Janjić. The step-mountain eta coordinate model: Further developments of the convection, viscous sublayer, and turbulence closure schemes. *Monthly Weather Review*, 122(5):927–945, 1994.

[29] W. T. Jewell. Effects of moving cloud shadows on electric utilities with dispersed solar photovoltaic generation. Technical report, Oklahoma State Univ., Stillwater (USA), 1986.

[30] J. S. Kain and J. M. Fritsch. Convective parameterization for mesoscale models: The kain-fritsch scheme. In *The representation of cumulus convection in numerical models*, pages 165–170. Springer, 1993.

[31] W. Kempton, F. M. Pimenta, D. E. Veron, and B. A. Colle. Electric power from offshore wind via synoptic-scale interconnection. *Proceedings of the National Academy of Sciences*, 107(16):7240–7245, 2010.

[32] J. Kleissl, M. Lave, M. Jamaly, and J.-L. Bosch. Aggregate solar variability. In *Power and Energy Society General Meeting, 2012 IEEE*, pages 1–3. IEEE, 2012.

[33] P. Lauret, J. Boland, and B. Ridley. Bayesian statistical analysis applied to solar radiation modelling. *Renewable Energy*, 49:124–127, 2013.

[34] X. Lu, M. B. McElroy, and J. Kiviluoma. Global potential for wind-generated electricity. *Proceedings of the National Academy of Sciences*, 106(27):10933–10938, 2009.

[35] M. R. Milligan and R. Artig. Choosing wind power plant locations and sizes based on electric reliability measures using multiple-year wind speed measurements. Technical report, National Renewable Energy Lab., Golden, CO (US), 1999.

[36] A. Mills. Implications of wide-area geographic diversity for short-term variability of solar power. *Lawrence Berkeley National Laboratory*, 2010.

[37] A. Molod, L. Takacs, M. Suarez, and J. Bacmeister. Development of the geos-5 atmospheric general circulation model: evolution from merra to merra2. *Geoscientific Model Development*, 8(5):1339–1356, 2015.

[38] F. Monforti, T. Huld, K. Bódis, L. Vitali, M. D'isidoro, and R. Lacal-Arántegui. Assessing complementarity of wind and solar resources for energy production in italy. a monte carlo approach. *Renewable Energy*, 63:576–586, 2014.

[39] National Aeronautics and Space —Administration. `https://gmao.gsfc.nasa.gov/reanalysis/MERRA-2/`.

[40] T. Nikolakakis and V. Fthenakis. The optimum mix of electricity from wind-and solar-sources in conventional power systems: Evaluating the case for new york state. *Energy Policy*, 39(11):6972–6980, 2011.

[41] J. Olauson and M. Bergkvist. Modelling the swedish wind power production using merra reanalysis data. *Renewable Energy*, 76:717–725, 2015.

[42] S. Pfenninger and I. Staffell. Long-term patterns of european pv output using 30 years of validated hourly reanalysis and satellite data. *Energy*, 114:1251–1265, 2016.

[43] F. Prohaska. The climate of argentina, paraguay and uruguay. *Climates of Central and South America*, 12:13–112, 1976.

[44] B. Ridley, J. Boland, and P. Lauret. Modelling of diffuse solar fraction with multiple predictors. *Renewable Energy*, 35(2):478–483, 2010.

[45] S. Saha, S. Moorthi, X. Wu, J. Wang, S. Nadiga, P. Tripp, D. Behringer, Y.-T. Hou, H.-y. Chuang, M. Iredell, et al. The ncep climate forecast system version 2. *Journal of Climate*, 27(6):2185–2208, 2014.

[46] T. K. Simonsen and B. G. Stevens. Regional wind energy analysis for the central united states. *Proc Global Wind Power*, page 16, 2004.

[47] G. Sinden. Characteristics of the uk wind resource: Long-term patterns and relationship to electricity demand. *Energy Policy*, 35(1):112–127, 2007.

[48] W. C. Skamarock and J. B. Klemp. A time-split nonhydrostatic atmospheric model for weather research and forecasting applications. *Journal of Computational Physics*, 227(7):3465–3485, 2008.

[49] W. C. Skamarock, J. B. Klemp, J. Dudhia, D. O. Gill, D. M. Barker, W. Wang, and J. G. Powers. A description of the advanced research wrf version 2. Technical report, National Center For Atmospheric Research Boulder Co Mesoscale and Microscale Meteorology Div, 2005.

[50] J. C. Smith, M. R. Milligan, E. A. DeMeo, and B. Parsons. Utility wind integration and operating impact state of the art. *IEEE transactions on power systems*, 22(3):900–908, 2007.

[51] I. Staffell and R. Green. How does wind farm performance decline with age? *Renewable energy*, 66:775–786, 2014.

[52] I. Staffell and S. Pfenninger. Using bias-corrected reanalysis to simulate current and future wind power output. *Energy*, 114:1224–1239, 2016.

[53] I. Staffell and S. Pfenninger. The increasing impact of weather on electricity supply and demand. *Energy*, 2017.

[54] G. Thompson, P. R. Field, R. M. Rasmussen, and W. D. Hall. Explicit forecasts of winter precipitation using an improved bulk microphysics scheme. part ii: Implementation of a new snow parameterization. *Monthly Weather Review*, 136(12):5095–5115, 2008.

[55] I. Van der Hoven. Power spectrum of horizontal wind speed in the frequency range from 0.0007 to 900 cycles per hour. *Journal of meteorology*, 14(2):160–164, 1957.

[56] Y.-H. Wan. Wind power plant behaviors: analyses of long-term wind power data. Technical report, National Renewable Energy Lab., Golden, CO (US), 2004.

[57] Y.-H. Wan. Primer on wind power for utility applications. Technical report, National Renewable Energy Laboratory (NREL), Golden, CO., 2005.

[58] Y.-h. Wan and B. K. Parsons. Factors relevant to utility integration of intermittent renewable technologies. Technical report, National Renewable Energy Lab., Golden, CO (United States), 1993.

[59] J. Widén. Correlations between large-scale solar and wind power in a future scenario for sweden. *IEEE transactions on sustainable energy*, 2(2):177–184, 2011.

[60] M. Wild, D. Folini, F. Henschel, N. Fischer, and B. Müller. Projections of long-term changes in solar radiation based on cmip5 climate models and their influence on energy yields of photovoltaic systems. *Solar Energy*, 116:12–24, 2015.

Tomás Guozden recieved his BS, MS and Ph.D degrees from the Instituto Balseiro, Bariloche, Argentina. After that he was employed

at CNEA, the National Atomic Energy Commission from Argentina. He worked mainly in numerical problems in the areas of electromagnetics, mechanical fracture and fluid dynamics. Since 2016 he is leading a project at Río Negro University (UNRN), aimed to support and develop renewable energy in Argentina. Currently his work and research interest are integration and forecasting of wind and solar energy.

Emilio Bianchi received the B.S. degree in atmospherical sciences from the Buenos Aires University and the Ph.D. in biology from the Comahue University. From 2009 to 2015 he worked as a researcher at the National Institute of Agricultural Technology of Argentina. He is currently a researcher and professor at the Río Negro University. His research interests include the link between large scale climatic features and renewable energy resources and the integration of renewable energies into the energy matrix.

Andrés Solarte received his B.S. in topographical engineering from the University of Valle, Colombia, in 2012. He is currently pursuing the M.S. degree in Emergency Early Warning and Response Space Applications at the National Committee of Space Activities of Argentina. Since 2016, he is currently working as a researcher at the Río Negro University. His research interests include spatial data processing and geographical information systems.

Juan Pablo Carbajal recieved his BS and MS degrees from the Instituto Balseiro, Bariloche, Argentina and his Ph.D from the University of Zürich, Switzerland. His interest in Complex Systems brought him into collaborations with professional in artificial intelligence, robotics, machine learning, biology, physics, and more; contributing with his expertise in modelling and analysis. Currently he leads the EmuMore project at the Swiss Federal Institute of Aquatic Science and Technology promoting the use of emulators in enviromental sciences.